

Phonon blockade effect in a coupled nonlinear mechanical system at finite temperature

Shengguo Guan¹, Warwick Bowen², Cunjin Liu¹, and Zhenglu Duan^{1*}

¹ *College of Physics, Communication and Electronics, Jiangxi Normal University, Nanchang, 330022, China and*

² *Center for Engineered Quantum Systems, School of Mathematics and Physics, The University of Queensland, St Lucia, Queensland 4072, Australia*

In this paper we study the unconventional phonon blockade effect in a coupled nonlinear micro/nanomechanical resonator system at finite temperature. The optimal condition for phonon antibunching is given by solving the stationary Liouville-Von Neumann master equation. We show that at low temperature the phonon blockade effect occurs even for extremely weak nonlinearity, which is confirmed by analytical and numerical solutions. We find that thermal noise degrades the blockade effect and that above a critical temperature the blockade effect completely disappears. However, we also find that a relative stronger driving force would help to preserve quantum correlation of the system against the thermal noise. Finally, we propose a nonclassical state of mechanical resonator d generation scheme based on our system with a pulsed driving force.

I. INTRODUCTION

Quantum state transfer and storage are crucial in quantum information processing. Up to now the most used information carrier to transfer and store quantum information is photon, which has the advantage of high velocity, being robust to environment, and good integrability. However, phonons, or vibrational modes of mechanical resonators, can be maintained a very long time before being eventually damped, and have the ability to interact with a wide range of quantum systems, such as electric, magnetic, and optical systems. Therefore, phonons have shown promising potential as quantum information carriers [1–3].

In quantum phononic networks, nonclassical state of phonon or a single phonon are important elements. Many methods to prepare nonclassical states of phonon or single phonon have been proposed. For example, A single phonon can be excited with a superconducting qubit from a mechanical resonator cooled down to a ground state [4]; a single-phonon Fock state is prepared by two-phonon damping [5]; A non-Gaussian states of mechanical resonator is generated by measurement [6]; Single phonon is produced by heralded measurement of the Stokes photon in cavity optomechanics [7, 8].

It is well known that, a sufficiently high kerr nonlinearity in an optical cavity will prevent further photons from entering once one photon occupies, which is called the photon blockade effect [9]. The transmitted light passing through the optical cavity then shows strong antibunching, which can be used to convert a coherent field into a train of single photons [10]. Similar to its optical counterpart, the phonon can also exhibit an antibunching effect in a strong nonlinear nanomechanical resonator [11–15]. However, the typical intrinsic nonlinearity of most micro/nanomechanical resonators is weak [16–19]. Thus, we would like to know whether a phonon blockade can be realized with weak nanomechanical nonlinearities.

In fact, a similar problem of weak nonlinearity also exists in the optical case. In an approach to address this problem,

Liew and Savona found that photons exhibit strong antibunching in a system consisting two coupled optical cavities with weak optical nonlinearity, which is named the unconventional photon blockade (UPB). Ciuti *et al* found that the underlying physics of UPB is that the excitation from the vacuum state to the two-photon state was prohibited by the destructive quantum interference between distinct pathways with a small and finite nonlinearity in the auxiliary cavity [20–23]. Owing to the high resonant frequency of an optical cavity, the thermal photon number is negligibly small at room temperature. Therefore the effect of thermal photons on the photon statistics and correlations is usually neglected safely. However, for mechanical resonators, the thermal phonon number is not negligible and has a significant influence on the phonon blockade even at milliKelvin temperature [12, 13, 24]. Hence, an analytical study of phonon blockade may help to give a deeper insight into the quantum correlation at finite temperature.

Motivated by these work above, we propose a scheme to realize unconventional phonon blockade by coupling a linear micro/nanomechanical resonator to a weakly nonlinear micro/nano-mechanical resonator. The optimal blockade conditions of this system are analytically found at finite temperature based on stationary Liouville-Von Neumann master equation. In particular, we systematically study the effect of the thermal noise on the blockade behavior. Finally, we investigate the time-dependent phonon blockade effect with a pulsed driving force. We expect our system can be used to generate a nonclassical phonon state.

This work is organized as follows. In Sec. II, we introduce our model and give the system Hamiltonian; then, we analytically and numerically study the phonon statistics at zero and finite temperatures in Sec. III; In Sec. IV we study the phonon blockade with a pulsed periodic driving signal and show its application in single-phonon generation; finally, we conclude our work in Sec. V.

II. MODEL

As shown in Fig. 1, the system under consideration consists of two linearly-coupled doubly-clamped mechanical beams. One mechanical beam contains a weak Duffing nonlinearity

arXiv:1708.01392v1 [quant-ph] 4 Aug 2017

[1] * duanzhenglu@jxnu.edu.cn

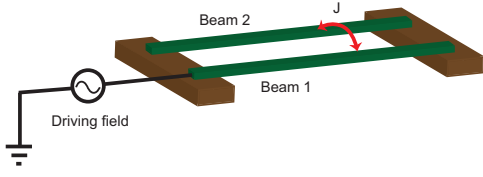


FIG. 1: (Color online) Schematic drawing of the phonon blockade effect. A linear mechanical beams, driven by an external force, is linearly coupled to another nonlinear mechanical beam.

and the other one is a linear resonator driven by a force signal. The mechanical nonlinearity can be intrinsic, such as geometric nonlinearity [16], or, it can be induced by coupling the mechanical oscillator to a low-dimensional auxiliary system, such as Cooper-pair boxes [25], polar molecules [26], and quantum dots [27]. The coupling between mechanical resonators could, for instance, be achieved by applying a voltage between two electrodes patterned on the beams, which gives rise to a static intermodal coupling [28]; or using a non-rigid anchor strain to mediate between the two beams [29]. Contrary to the latter case, dielectric intermode coupling can be tuned freely.

We start from the classical equations of motion for the described coupled mechanical system

$$\frac{dp_1}{dt} = -\omega_1 x_1 - \gamma_1 p_1 + J(x_2 - x_1) + F \cos(\omega_d t), \quad (1)$$

$$\frac{dx_1}{dt} = \omega_1 p_1 \quad (2)$$

$$\frac{dp_2}{dt} = -\gamma_2 p_2 - \omega_2 x_2 + J(x_1 - x_2) + U x_2^3, \quad (3)$$

$$\frac{dx_2}{dt} = \omega_2 p_2 \quad (4)$$

where x_j and p_j ($j = 1, 2$), respectively, are the displacement and momentum of the j -th mechanical resonator with resonance frequency ω_j and damp rate γ_j . J is the coupling strength between two resonators and U is the nonlinearity strength of the mechanical resonator 2. We assume the resonator 1 is harmonically driven at frequency ω_d with amplitude F .

Now we introduce the phonon annihilation ($\hat{b}_j = (x_j + ip_j) / \sqrt{2}$) and creation ($\hat{b}_j^\dagger = (x_j - ip_j) / \sqrt{2}$) operators, which satisfy the commutators $[\hat{b}_j, \hat{b}_k^\dagger] = \delta_{jk}$. In the rotating frame of the driving frequency ω_d , the Hamiltonian governing the system in the quantum-mechanical frame is ($\hbar = 1$):

$$H = \Delta_1 \hat{b}_1^\dagger \hat{b}_1 + \Delta_2 \hat{b}_2^\dagger \hat{b}_2 + J(\hat{b}_1^\dagger + \hat{b}_1)(\hat{b}_2 + \hat{b}_2^\dagger) + F(\hat{b}_1^\dagger + \hat{b}_1) + U(\hat{b}_2 + \hat{b}_2^\dagger)^4 \quad (5)$$

with the detuning $\Delta_j = \omega_j - \omega_d$. For simplicity, in the following we assume the mechanical resonators share the same frequency and decay rate, i.e., $\Delta_1 = \Delta_2 = \Delta$ and $\gamma_1 = \gamma_2 = \gamma$. By neglecting the anti-rotating wave terms, the Hamiltonian Eq. (6) becomes

$$H = \Delta \hat{b}_1^\dagger \hat{b}_1 + \Delta \hat{b}_2^\dagger \hat{b}_2 + J(\hat{b}_1^\dagger \hat{b}_2 + \hat{b}_2^\dagger \hat{b}_1) + F(\hat{b}_1^\dagger + \hat{b}_1) + U \hat{b}_2^{\dagger 2} \hat{b}_2^2. \quad (6)$$

Hamiltonian (6) describes a model of driven-dissipative coupled nonlinear mechanical resonators, similar with the optical counterpart in Ref. [23]. This Hamiltonian is the starting point of our calculation.

III. RESULTS FOR PHONON BLOCKADE

In this section we investigate the phonon blockade at zero and finite temperatures. Unlike the situation of photon blockade, the environment temperature usually has a significant influence on typical phonon statistics and correlation, due to the low energy of single phonons. With the inclusion of the temperature factor, here we use the Liouville-Von Neumann master equation for the density matrix

$$\begin{aligned} \frac{d\hat{\rho}}{dt} &= \hat{L}\hat{\rho} \\ &= -i[H, \hat{\rho}] + \sum_{n=1,2} \frac{\gamma}{2} \left[(n_{th} + 1) D[\hat{b}_n] \hat{\rho} + n_{th} D[\hat{b}_n^\dagger] \hat{\rho} \right] \end{aligned} \quad (7)$$

with Lindblad operator $D[\hat{A}] \hat{\rho} = 2\hat{A}\hat{\rho}\hat{A}^\dagger - \hat{A}^\dagger\hat{A}\hat{\rho} - \hat{\rho}\hat{A}^\dagger\hat{A}$. Here $n_{th} = (\exp(T_0/T) - 1)^{-1}$ is the average phonon number of the mechanical resonators at the temperature T (We assume that the temperatures of two nanomechanical beams are the same), and $T_0 = \hbar\omega/K_B$ is the characteristic temperature of the system with the Boltzmann constant K_B .

In this situation, the statistic properties of phonons for mechanical beam 1 is described by the equal-time second-order correlation function:

$$g^{(2)}(0) = \frac{\text{Tr}(\hat{b}_1^\dagger \hat{b}_1^\dagger \hat{b}_1 \hat{b}_1 \hat{\rho}_{ss})}{\text{Tr}(\hat{b}_1^\dagger \hat{b}_1 \hat{\rho}_{ss})^2} \quad (8)$$

where $\hat{\rho}_{ss}$ is the steady-state density matrix by setting $d\hat{\rho}/dt = 0$ in Eq. (7). In the calculation we write $\hat{\rho}$ as the density matrix $\hat{\rho} = \sum_{m,n=0}^{\infty} \rho_{mn,m'n'} |mn\rangle \langle m'n'|$ on the basis of phonon number states $|mn\rangle$, where m denotes the phonon number in mechanical mode 1 and n denotes the phonon number in mechanical mode 2. To find the steady-state density matrix, one need to find the eigen matrix $\hat{\rho}_{ss}$ of superoperator \hat{L} when it has an eigenvalue of 0, i.e., $\hat{L}\hat{\rho} = \lambda\hat{\rho}$ ($\lambda = 0$).

A. Zero temperature case

Fig. 2 shows the numerical result of the equal-time second-order correlation function as a function of the nonlinearity U and mechanical coupling J at zero temperature. We can see that the phonon antibunching effect occurs in the parameter regime where the product JU is relatively small. Importantly, different from the conventional phonon blockade effect, in this coupled-mechanical oscillator system phonons exhibit antibunching even when the nonlinearity is vanishingly small ($U \ll \gamma$), although at the cost of a large J . In addition, in the regime of large U and J , $g^{(2)}(0)$ becomes extremely large, which means that phonons are superbunched.

To find the optimal condition for phonon antibunching, we analytically solve the steady-state master equation for the density matrix. Under the weak driving condition $F \ll \gamma$, the average mechanical excitations would be much lower than 1 and the Hilbert space of the total system can be truncated to $m + n = 2$. In this case, we denote $|0, 0\rangle \rightarrow |1\rangle$, $|0, 1\rangle \rightarrow |2\rangle$, $|0, 2\rangle \rightarrow |3\rangle$, $|1, 0\rangle \rightarrow |4\rangle$, $|1, 1\rangle \rightarrow |5\rangle$, and $|2, 0\rangle \rightarrow |6\rangle$. Hence the density matrix operator $\hat{\rho}$ can be written as $\hat{\rho} = \sum_{m,n=1}^6 \rho_{mn} |m\rangle \langle n|$. Additionally, weak mechanical excitations would result in $\rho_{00} \gg \rho_{01}, \rho_{10} \gg \rho_{02}, \rho_{20}, \rho_{11}$. Then the equal-time second-order correlation function can be approximately expressed as:

$$g^{(2)}(0) \simeq \frac{2\rho_{66}}{\rho_{44}^2}, \quad (9)$$

Obviously, if $\rho_{66} = 0$, then $g^{(2)}(0) = 0$, which implies a vanishing probability of having two phonons in the first mechanical mode. After tedious calculation using the perturbation theory (as shown in Appendix), we obtain the expression for the matrix element ρ_{66} in the zero temperature case ($n_{th} = 0$)

$$\rho_{66} = \frac{F^4 |U(J^2 + 2\tilde{\Delta}^2) + 2\tilde{\Delta}^3|^2}{2J^8 |U + 2\tilde{\Delta}|^2}. \quad (10)$$

where $\tilde{\Delta} = \Delta - i\gamma/2$. Then we can find the following condition for perfect antibunching

$$U(J^2 + 2\tilde{\Delta}^2) + 2\tilde{\Delta}^3 = 0 \quad (11)$$

i.e.

$$2UJ^2 + 4(\Delta + U)\Delta^2 - (3\Delta + U)\gamma^2 = 0 \quad (12)$$

$$8U\Delta + 12\Delta^2 - \gamma^2 = 0 \quad (13)$$

which is mathematically the same as the results in the photon blockade case [23]. We plot the optimal condition in Fig. 2 (white dashed curve), which is well consistent with the numerical result.

In the situation where the mechanical coupling J is far greater than the mechanical damping γ , the optimal parameters to achieve $\rho_{66} = 0$ can be approximated as

$$\Delta_{optimal} \simeq \frac{\gamma}{2\sqrt{3}} \quad (14)$$

$$U_{optimal} \simeq \frac{2\gamma^3}{3\sqrt{3}J^2} \quad (15)$$

Obviously, in this situation the required nonlinearity to observe optimal blockade can be made extremely small ($U_{optimal}/\gamma = 2\gamma^2/(3\sqrt{3}J^2) \ll 1$), contrary to the condition of conventional phonon blockade ($U/\gamma \gg 1$).

We then study the phonon number probability distribution $P_m = \sum_{n=0}^{\infty} \rho_{mn, mn}$ of mechanical mode 1 when the phonon blockade occurs. For comparison, we also show the probability distribution of a coherent state with the same mean phonon

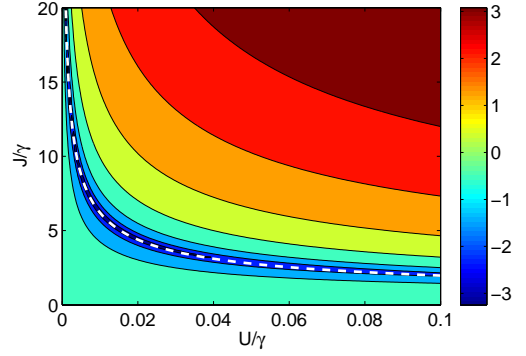


FIG. 2: (Color online) Equal-time second-order correlation function $\log_{10}(g^{(2)}(0))$ as a function of the mechanical coupling J and the nonlinear coefficient U at zero temperature. The white dashed curve is calculated from the analytical optimal conditions Eqs. (12) and (13). The parameters are: $\gamma = 1$, $\Delta = 0.29\gamma$, and $F = 0.001\gamma$.

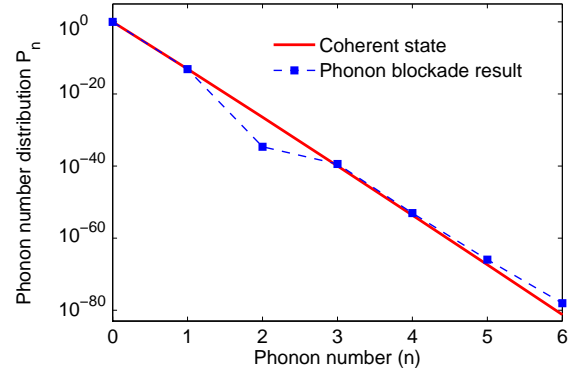


FIG. 3: (Color online) Population distribution of number state of phonon mode 1. The other parameters are: $\gamma = 1$, $U = 0.00387\gamma$, $J = 10\gamma$, $\Delta = 0.2874\gamma$, and $F = 0.00005\gamma$.

number $|\alpha|^2 = \sum_{m=0}^{\infty} P(m)$, which obeys the Poisson distribution $P(n) = |\alpha|^{2n} e^{-|\alpha|^2} / n!$. As shown in Fig. 3, the largest probability is occupied by the vacuum state. The one-phonon state is next most probable. The two-phonon state is dramatically less probable than the single-phonon state. Compared to the coherent state (the same mean phonon number with the blockade case), the probability for two-phonon state is apparently, which indicates that the state of the mechanical mode 1 has a nonclassical distribution.

B. Finite temperature case

In the previous subsection we studied the phonon blockade effect without including the effect of environmental temperature. However, cooling a mechanical resonator down to zero temperature is not easy experimentally. Therefore, it is important to study the phonon blockade at finite temperature. We first numerically plot $g^{(2)}(0)$ as a function of J and U at $T = 0.04T_0$ in Fig. 4. The phonon antibunching effect still

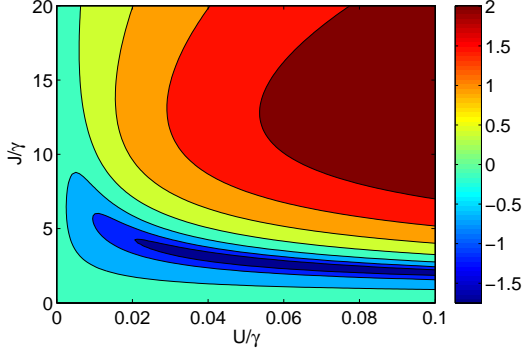


FIG. 4: (Color online) Equal-time second-order correlation function $\log_{10}(g^{(2)}(0))$ as a function of tunnel coupling J and nonlinearity U at the temperature $T = 0.04T_0$. It is plotted in the logarithmic scale. The other parameters are: $\gamma = 1$, $\Delta = 0.29\gamma$ and $F = 0.001\gamma$.

exists in the weak nonlinearity limit. However, in the low U and large J regime $g^{(2)}(0)$ is higher than that at zero temperature (See Fig. 2), although it is still below 1. This indicates that the thermal noise degrades the blockade effect.

To study the effect of the environmental temperature on the phonon blockade, we present the approximate analytical expressions of the density matrix elements ρ_{66} and ρ_{44} in the strong coupling regime (see Appendix):

$$\rho_{44} = \frac{F^2 |\tilde{\Delta}|^2}{|J^2 - \tilde{\Delta}^2|^2} + n_{th} \quad (16)$$

$$\rho_{66} = \frac{F^4 |U(J^2 + 2\tilde{\Delta}^2) + 2\tilde{\Delta}^3|^2}{2J^8 |U + 2\tilde{\Delta}|^2} + \frac{2F^2 |\tilde{\Delta}|^2}{J^4} n_{th} + n_{th}^2 \quad (17)$$

From Eqs. (16-17), both ρ_{44} and ρ_{66} contain two parts: one part determined by the temperature or the thermal phonon number and the other part from the system itself. These two parts incoherently contribute to the phonon correlation. From Eq. (17), one can note that $\rho_{66} > 0$, which implies that the perfect antibunching condition no longer exists for finite temperature. When the environmental temperature is small, the region for $0 < g^{(2)}(0) < 1$ still exists because the system interference partially contributing to phonon correlation leads to an imperfect antibunching effect. These conclusions are well confirmed by the numerical results in Fig. 4.

Fig. 5 shows $g^{(2)}(0)$ as a function of the environment temperature, with near perfect agreement between numerical results and analytical results. When the temperature is below a value of $T_{c1} = 0.033T_0$, the second-order correlation function remains far beneath 1. In this regime, the phononic mode remains strong antibunching. When $T > T_{c1}$, $g^{(2)}(0)$ experiences a sharp increase. $g^{(2)}(0)$ approaches a value of 2 at a second critical temperature $T_{c2} = 0.0463T_0$, which indicates that the phononic mode has the statistic property of thermal field. This behaviour can be explained from Eq. (17): at a low temperature the first term of Eq. (17) (the quantum interference term) dominates and $g_2^{(0)}$ is very small. With increasing temperature, the thermal noise becomes important. When the

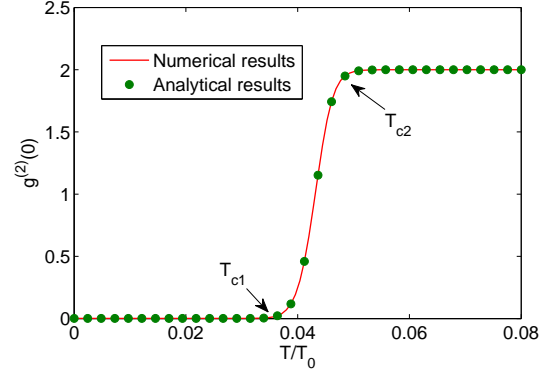


FIG. 5: (Color online) Equal-time second-order correlation function $g^{(2)}(0)$ as a function of environmental temperature T . The coupling strength $J = 20\gamma$ and nonlinearity $U = 0.001\gamma$. The numerical result is obtained based on Eq. (8) and the analytical result is calculated from Eqs. (9) and (16-17). Two threshold temperatures are $T_{c1} = 0.033T_0$ and $T_{c2} = 0.0463T_0$. The other parameters are: $\gamma = 1$, $\Delta = 0.29\gamma$, and $F = 0.01\gamma$.

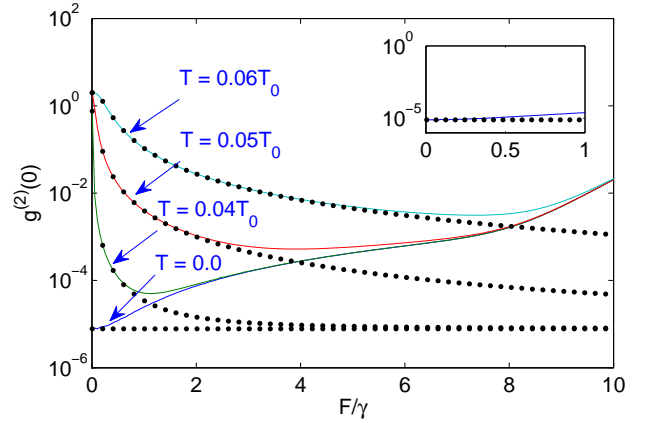


FIG. 6: (Color online) Equal-time second order correlation function $g^{(2)}(0)$ versus the driving strength F at different temperatures. The dot represent analytical results and the solid line are the numerical results. The inset is the zero temperature case. The other parameters are: $\gamma = 1$, $U = 0.00096\gamma$, $J = 20\gamma$, $\Delta = 0.2885\gamma$.

temperature rises to a critical temperature T_{c1} , the first term is equal to the second term and greater than the third term, i.e., $n_{th,1} = \frac{F^2 |U(J^2 + 2\tilde{\Delta}^2) + 2\tilde{\Delta}^3|^2}{4J^4 |U\tilde{\Delta} + 2\tilde{\Delta}^2|^2}$. When $T > T_{c1}$, the quantum interference term contributes less than the thermal terms. When the temperature reaches T_{c2} , the third term is equal to the second term and much greater than the quantum interference term, i.e., $n_{th,2} = 2 |F\tilde{\Delta}/J^2|^2$. When $T > T_{c2}$, the pure thermal noise term dominates the system and one can easily find $g^{(2)}(0) \approx 2$. The underlying physics is that the strong thermal noise can destroy the quantum correlation of the phonon mode. Therefore, a relatively low temperature is required to experimentally observe the phonon blockade.

We then investigate the influence of the driving force amplitude on the phonon statistics. In Fig. 6 we plot $g^{(2)}(0)$ of beam 1 as a function of the driving force at four different

temperatures. One can see that $g^{(2)}(0)$ in each curve at finite temperature firstly decreases and then increases as the driving force is increased. In the weak driving limit, the analytical model well reproduces the more complete numerical calculation. However, since it is truncated to small phonon number, it fails to reproduce the increasing $g^{(2)}(0)$ at higher driving. Note that, for higher environmental temperatures, a stronger driving is needed to reach an optimal phonon antibunching effect. These observations can be understood from Eqs. (16) and (17). When F is very small, the thermal noise dominates the matrix elements ρ_{44} and ρ_{66} and hence the phonon state is approximately the thermal state ($g^{(2)}(0) \approx 2$). With the increase in driving strength, the contributions from the quantum interference terms in Eqs. (16) and (17) become important, leading to a decrease in $g^{(2)}(0)$. When the driving is strong enough, the three and higher phonon states in resonator 1 are populated with increased probability owing to the coupling with resonator 2. Hence, the second correlation function will increase, which leads to a degradation of phonon antibunching. For the zero temperature case, the second-order correlation function is

$$g^{(2)}(0) = \left| \frac{(U(J^2 + 2\tilde{\Delta}^2) + 2\tilde{\Delta}^3)|J^2 - \tilde{\Delta}^2|^2}{(U + 2\tilde{\Delta})|\tilde{\Delta}|^2 J^4} \right|^2. \quad (18)$$

One can see that $g^{(2)}(0)$ is independent on F , which is verified by the approximate analytic result in Fig. (6). The numeric result shows that $g^{(2)}(0)$ remains constant for a small driving force and monotonously increases for a further increased temperature. From the discussions above it is clear that a suitable driving strength is helpful to preserve better phonon blockade effect when thermal noise exists and for zero temperature a very weak force is required to achieve better blockade effect.

Now we discuss the experimental feasibility to observe the phonon blockade effect in the presence of unavoidable thermal noise. The typical frequency of the nanomechanical resonator is in the range of GHz (i.e., 5.6 GHz in Ref. [30]) and the corresponding character temperature $T_0 = \hbar\omega/K_B \sim 40$ mK. According to the discussion above, when the environmental temperature is below 1.32 mK, the phonon blockade is almost unaffected by the thermal noise. Such a temperature is available with current laboratory technology.

IV. NONCLASSICAL PHONON STATE GENERATION BY PULSED EXCITATION

Nonclassical states of the mechanical resonator play an important role in quantum information, foundation test of quantum mechanics and of the nature of entanglement [1–3]. Here we propose a feasible protocol to generate a train of phonon pulses in the nonclassical state by applying a periodic external driving based on unconventional phonon blockade discussed in previous sections. Similar protocols have been proposed in generating nonclassical states of light [31] and single photons [32].

We assume that our system is driven by a train of periodic Gaussian pulses ($F = F_0 \sum_n \exp(-(t - t_0 - n\tau)^2/t_{width}^2)$),

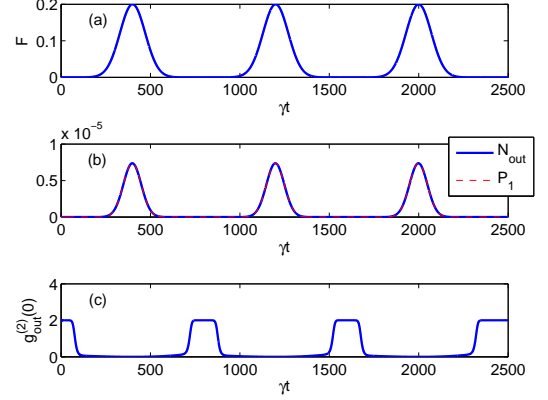


FIG. 7: (Color online) Single phonon excitation induced by a periodic Gaussian pulse force. (a) is the time sequence of driving force; (b) show the mean output phonon number and the amplitude of single phonon; (c) is the equal time second order correlation dependent on time. The other parameters are: $\gamma = 1$, $U = 0.009\gamma$, $J = 6.5\gamma$, $\Delta = 0.2857\gamma$, $\gamma t_0 = 400$, $\gamma\tau = 100$, and $T = 0.03T_0$.

where F_0 is the driving strength, t_{width} is the pulse width and τ is the interval between Gaussian pulses. To avoid interference between pulses, the time intervals should exceed the characteristic time of dissipative processes, i.e., $\tau \gg \gamma^{-1}$. Also, enough large pulse width is needed to avoid the nonadiabatic phonon excitation. Here we assume $t_{width} \gg \gamma^{-1}$.

For a practically feasible nonclassical phonon field source, an output export is required. Following the structure in Refs. [31, 33], we assume that the resonator 1 has two input-output channels with decay rates γ_a and γ_b ($\gamma = \gamma_a + \gamma_b$). The strong external driving F is acted on channel a while the input of channel b is the vacuum. With the assumption that the decay rates $\gamma_a \ll \gamma_b \approx \gamma$, the generated phonons almost leak into channel b . According to the input-output relation [34, 35], the output phonon model can be expressed as

$$\hat{b}_{out} = \hat{b}_{in} + \sqrt{\gamma_b} \hat{b}_1 \quad (19)$$

with vacuum noise operator \hat{b}_{in} and the corresponding output mean phonon number is

$$\begin{aligned} N_{out} &= \langle \hat{b}_{out}^\dagger \hat{b}_{out} \rangle \\ &= \gamma_b \langle \hat{b}_1^\dagger \hat{b}_1 \rangle \end{aligned} \quad (20)$$

Since we have taken the assumption that the only vacuum noise is input from channel b , there is no correlation between the intra cavity mode and the input noise. The phonon pulse emitted from the output port can be analyzed by using a single-phonon counter [36]. The emitted phonon field can be expressed in the Fock basis as $|b_{out}\rangle = \sum_{m=0}^{\infty} C_m |m\rangle$. Below we will show in certain parameter region every emitted phonon pulse exhibits strong nonclassicality and the probabilities of the two-phonon and multi-phonon states almost vanish.

In Fig. 7, the system responses under a periodic pulsed driving at the temperature $T = 0.03T_0$ are presented. Fig. 7 (a)

shows the input periodic driving and (b) are the time evolution of the mean output phonon number (N_{out} , blue solid curve) and the emitted single-phonon probability (P_1 , the red dashed curve). It is seen that the amplitude and shape of the emitted single-phonon probability is almost equivalent to those of the mean output phonon number.

To quantitatively evaluate the quantum statistics and correlation of the emitted phonon field, we also calculate the time-dependent equal-time second-order correlation function:

$$g_{\text{out}}^{(2)}(t, 0) = \frac{\text{Tr}(\hat{b}_{\text{out}}^{\dagger 2} \hat{b}_{\text{out}}^2 \hat{\rho}(t))}{\text{Tr}(\hat{b}_{\text{out}}^{\dagger} \hat{b}_{\text{out}} \hat{\rho}(t))^2} \quad (21)$$

Fig. 7 (c) shows the nonstationary second-order correlation function $g_{\text{out}}^{(2)}(t, 0)$ versus time. It is clear that the emitted phonon pulse has strong antibunching effect since the corresponding $g_{\text{out}}^{(2)}(t, 0)$ is nearly zero. Therefore, we can say that the emitted phonon field does not include two-phonon and multi-phonon states and has a strong nonclassicality. The emitted phonon field can be approximately expressed as $|b_{\text{out}}\rangle \simeq C_0|0\rangle + C_1|1\rangle$. It is worthy to note that, in each emitted phonon pulse the single phonon probability $|C_1|^2$ is very small, hence the efficiency for generating single-phonon would be low and further investigation for improve efficiency is required. Further, in the time intervals between driving pulses, $g_{\text{out}}^{(2)}(t, 0) \approx 2$. This is because the thermal noise dominates the phonon correlation when the driving is weak, as discussed in last section. Nevertheless, we put forward a scheme to realize the generation of a nonclassical state of phonon field with weak mechanical nonlinearity.

V. CONCLUSION

We have studied the phonon blockade effect in a coupled mechanical system with weak mechanical nonlinearity at both zero and finite temperatures. Analytical results have been derived for the phonon antibunching and investigating the temperature effect on phonon blockade based on the stationary master equation. The optimal condition is coincident to that solved by the wave function method. When the thermal noise exists, the perfect antibunching condition is destroyed, leading to a finite blockade to the mechanical mode. We find the thermal noise has a negligibly small influence on the quantum statistics of the phonon mode when the environmental temperature is below a critical value. The effect of the driving force on the phonon blockade is also examined. It is found that a relatively strong driving would help to preserve a better phonon blockade effect at finite temperature as it not far strong. In addition, we have studied the blockade effect with a periodic pulsed driving signal and shown its application in nonclassical phonon state generation.

Acknowledgments

This work is supported by the National Natural Science Foundation of China under Grants No. 11364021

and No.11664014, Natural Science Foundation of Jiangxi Province under Grants 20161BAB201023. W.P. Bowen acknowledges support from the Australian Research Council through grants CE110001013 and FT140100650.

Appendix A

In this appendix we will show how to calculate the density matrix elements for stationary state at finite temperature. To find the steady-state density matrix, we need to find the eigenmatrix $\hat{\rho}_{ss}$ of superoperator \hat{L} when it has an eigenvalue of 0, i.e., $\hat{L}\hat{\rho} = \lambda\hat{\rho}$ ($\lambda = 0$), where we can truncate the phononic Hilbert space to $N_{\text{tot}} = 2$. We expand the matrix equation and obtain a coupled equations for the density matrix elements. In the weak driving limit, we can divide the set of the coupled equations into several sets according to the orders of F/γ . The zeroth-order equation is $\rho_{11} = 0$. The first-order equations are

$$0 = J\rho_{41} + (\Delta - i\gamma/2)\rho_{21} \quad (\text{A1})$$

$$0 = J\rho_{21} + (\Delta - i\gamma/2)\rho_{41} + E\rho_{11} \quad (\text{A2})$$

The second-order equations are

$$0 = J\rho_{51} + \sqrt{2}(U + \Delta - i\gamma/2)\rho_{31} \quad (\text{A3})$$

$$0 = J\rho_{31} + \sqrt{2}(\Delta - i\gamma/2)\rho_{61} + E\rho_{41} \quad (\text{A4})$$

$$0 = \sqrt{2}J(\rho_{31} + \rho_{61}) + 2(\Delta - i\gamma/2)\rho_{51} + E\rho_{21} \quad (\text{A5})$$

$$0 = J(\rho_{22} - \rho_{44}) - i\gamma\rho_{42} + E\rho_{12} \quad (\text{A6})$$

$$0 = E(\rho_{41} - \rho_{14}) + i\gamma(\rho_{22} + \rho_{44}) - 2i\gamma n_{\text{th}}\rho_{11} \quad (\text{A7})$$

$$0 = J(\rho_{42} - \rho_{24}) - i\gamma\rho_{22} + E(\rho_{52} - \rho_{25}) + i\gamma n_{\text{th}}\rho_{11} \quad (\text{A8})$$

$$0 = J(\rho_{24} - \rho_{42}) - i\gamma\rho_{44} + E(\rho_{14} - \rho_{41}) + i\gamma n_{\text{th}}\rho_{11} \quad (\text{A9})$$

The third-order equations are

$$0 = \sqrt{2}J\rho_{52} - J\rho_{64} + (\Delta - 3i\gamma/2)\rho_{62} + \sqrt{2}E\rho_{42} \quad (\text{A10})$$

$$0 = J\rho_{23} - \sqrt{2}J\rho_{45} - (2U + \Delta + 3i\gamma/2)\rho_{43} + E\rho_{13} \quad (\text{A11})$$

$$0 = \sqrt{2}J\rho_{52} - J\rho_{34} + (2U + \Delta - 3i\gamma/2)\rho_{32} + \sqrt{2}i\gamma n_{\text{th}}\rho_{21} \quad (\text{A12})$$

$$0 = \sqrt{2}J\rho_{32} + \sqrt{2}J\rho_{62} - J\rho_{54} + (\Delta - 3i\gamma/2)\rho_{52} + E\rho_{22} + i\gamma n_{\text{th}}\rho_{41} \quad (\text{A13})$$

$$0 = \sqrt{2}J\rho_{54} - J\rho_{62} + (\Delta - 3i\gamma/2)\rho_{64} + \sqrt{2}E\rho_{44} - E\rho_{61} - \sqrt{2}i\gamma n_{\text{th}}\rho_{41} \quad (\text{A14})$$

$$0 = \sqrt{2}J\rho_{34} + \sqrt{2}J\rho_{64} - J\rho_{52} + (\Delta - 3i\gamma/2)\rho_{54} + E\rho_{24} - E\rho_{51} + i\gamma n_{\text{th}}\rho_{21} \quad (\text{A15})$$

The fourth-order equations are

$$0 = \sqrt{2}J(\rho_{53} - \rho_{35}) - 2i\gamma\rho_{33} + 2i\gamma n_{th}\rho_{22} \quad (\text{A16})$$

$$0 = \sqrt{2}J(\rho_{53} - \rho_{65}) - 2(U + i\gamma)\rho_{63} + \sqrt{2}E\rho_{43} \quad (\text{A17})$$

$$0 = \sqrt{2}J(\rho_{56} - \rho_{65}) - 2i\gamma\rho_{66} + \sqrt{2}E(\rho_{46} - \rho_{64}) + 2i\gamma n_{th}\rho_{44} \quad (\text{A18})$$

$$0 = \sqrt{2}J(\rho_{55} - \rho_{63} - \rho_{66}) - 2i\gamma\rho_{65} - E\rho_{62} + \sqrt{2}E\rho_{45} + \sqrt{2}i\gamma n_{th}\rho_{42} \quad (\text{A19})$$

$$0 = \sqrt{2}J(\rho_{33} - \rho_{55}) + \sqrt{2}J\rho_{63} - 2(U + i\gamma)\rho_{53} + E\rho_{23} + \sqrt{2}i\gamma n_{th}\rho_{42} \quad (\text{A20})$$

$$0 = \sqrt{2}J(\rho_{35} - \rho_{53}) + \sqrt{2}J(\rho_{65} - \rho_{56}) - 2i\gamma\rho_{55} + E(\rho_{25} - \rho_{52}) + i\gamma n_{th}(\rho_{22} + \rho_{44})$$

We first find the solutions first-order equations (A1) and (A2):

$$\rho_{14}^* = \rho_{41} = \frac{E\tilde{\Delta}}{J^2 - \tilde{\Delta}^2} \quad (\text{A21})$$

$$\rho_{12}^* = \rho_{21} = -\frac{JE}{J^2 - \tilde{\Delta}^2} \quad (\text{A22})$$

here we have denoted $\tilde{\Delta} = \Delta - i\gamma/2$. Then we substitute Eqs. (A21) and (A22) into Eqs. (A5)-(A9) and obtain the solutions for the second order equations:

$$\rho_{22} = \frac{J^2 E^2}{|J^2 - \tilde{\Delta}^2|^2} + n_{th} \quad (\text{A23})$$

$$\rho_{44} = \frac{E^2 |\tilde{\Delta}|^2}{|J^2 - \tilde{\Delta}^2|^2} + n_{th} \quad (\text{A24})$$

$$\rho_{24}^* = \rho_{42} = -\frac{JE^2\tilde{\Delta}}{|J^2 - \tilde{\Delta}^2|^2} \quad (\text{A25})$$

$$\rho_{16}^* = \rho_{61} = \frac{\sqrt{2}E^2(U(J^2 + 2\tilde{\Delta}^2) + 2\tilde{\Delta}^3)}{2(J^2 - \tilde{\Delta}^2)^2(U + \tilde{\Delta})} \quad (\text{A26})$$

$$\rho_{13}^* = \rho_{31} = \frac{\sqrt{2}\tilde{\Delta}J^2E^2}{(J^2(U + 2\tilde{\Delta}) - 2\tilde{\Delta}^2(U + \tilde{\Delta}))(J^2 - \tilde{\Delta}^2)} \quad (\text{A27})$$

$$\rho_{15}^* = \rho_{51} = -\frac{2(U + \tilde{\Delta})\tilde{\Delta}JE^2}{(J^2(U + 2\tilde{\Delta}) - 2\tilde{\Delta}^2(U + \tilde{\Delta}))(J^2 - \tilde{\Delta}^2)} \quad (\text{A28})$$

Using the same procedure, we can also find solutions for other higher order equations after long iteration. The third-order solutions are

$$\rho_{25}^* = \rho_{52} = -\frac{\tilde{\Delta}E^3}{|J^2 - \tilde{\Delta}^2|^2} - \frac{E\tilde{\Delta}}{J^2}n_{th} \quad (\text{A29})$$

$$\rho_{23}^* = \rho_{32} = -\frac{E^3(J^2 - \tilde{\Delta}^2)}{\sqrt{2}J|J^2 - \tilde{\Delta}^2|^2} - \frac{\sqrt{2}EJ}{(J^2 - \tilde{\Delta}^2)}n_{th} \quad (\text{A30})$$

$$\rho_{26}^* = \rho_{62} = -E^3\frac{U(J^2 + 2\tilde{\Delta}^2) + 2\tilde{\Delta}^3}{2\sqrt{2}\tilde{\Delta}J^5} + \frac{E^2(\Delta - 3i\gamma/2)}{6J^3} \quad (\text{A31})$$

$$\rho_{45}^* = \rho_{54} = -\frac{E^3|\tilde{\Delta}|^2}{J|J^2 - \tilde{\Delta}^2|^2} - \frac{E}{J}n_{th} \quad (\text{A32})$$

$$\rho_{46}^* = \rho_{64} = \frac{E^3\tilde{\Delta}^*(U(J^2 + 2\tilde{\Delta}^2) + 2\tilde{\Delta}^3)}{2\sqrt{2}\tilde{\Delta}J^6} + \frac{\sqrt{2}E\tilde{\Delta}}{J^2}n_{th} \quad (\text{A33})$$

$$\rho_{43}^* = \rho_{34} = \frac{\sqrt{2}E^3|\tilde{\Delta}|^2}{(U + 2\tilde{\Delta})|(J^2 - \tilde{\Delta}^2)|^2} + \frac{E^2}{J^2}n_{th} \quad (\text{A34})$$

Fourth-order solution are

$$\rho_{33} = \frac{|\tilde{\Delta}|^2 E^4}{2|(U + \tilde{\Delta}^*)(J^2 - \tilde{\Delta}^2)|^2} + n_{th}^2 \quad (\text{A35})$$

$$\rho_{55} = \frac{E^4|\Delta + i\gamma/2|^2}{J^2|(J^2 - \tilde{\Delta}^2)|^2} + n_{th}^2 \quad (\text{A36})$$

$$\rho_{66} = \frac{E^4}{2J^8}\left|\frac{U(J^2 + 2\tilde{\Delta}^2) + 2\tilde{\Delta}^3}{U + 2\tilde{\Delta}}\right|^2 + \frac{2E^2|\tilde{\Delta}|^2}{J^4}n_{th} + n_{th}^4 \quad (\text{A37})$$

$$\rho_{35}^* = \rho_{53} = -\frac{E^4|\tilde{\Delta}|^2}{\sqrt{2}J(U + \tilde{\Delta}^*)(J^2 - \tilde{\Delta}^2)|^2} - \frac{\sqrt{2}E^2\tilde{\Delta}}{J^3}n_{th} \quad (\text{A38})$$

$$\rho_{56}^* = \rho_{65} = -\frac{E^4\tilde{\Delta}^*(U(J^2 + 2\tilde{\Delta}^2) + 2\tilde{\Delta}^3)}{2\sqrt{2}J^5(J^2 - \tilde{\Delta}^2)\tilde{\Delta}} - \frac{\sqrt{2}E^2\tilde{\Delta}}{J^3}n_{th} \quad (\text{A39})$$

$$\rho_{36}^* = \rho_{63} = \frac{E^4(U(J^2 + 2\tilde{\Delta}^2) + 2\tilde{\Delta}^3)}{4\tilde{\Delta}J^6} - \frac{2U\tilde{\Delta}E^2}{J^4}n_{th} \quad (\text{A40})$$

- [1] S.J. Habraken, K. Stannigel, M.D. Lukin, P. Zoller, and P. Rabl, New Journal of Physics, **14**, 115004 (2012).
 [2] M.V. Gustafsson, T. Aref, A.F. Kockum, M.K. Ekstrom, G. Johansson, and P. Delsing, Science **346**, 207 (2014).
 [3] S. Rips and M.J. Hartmann, Phys. Rev. Lett. **110**, 120503 (2013).
 [4] A.D. Connell, M. Hofheinz, M. Ansmann, R.C. Bialczak, M. Lenander, E. Lucero, M. Neeley, D. Sank, H. Wang, M. Weides, J. Wenner, J.M. Martinis, and A.N. Cleland, Nature, **464**, 697

- (2010).
 [5] K. Borkje, Phys. Rev. A **90**, 023806 (2014).
 [6] M.R. Vanner, I. Pikovski, G.D. Cole, M.S. Kim, C. Brukner, K. Hammerer, G.J. Milburn, and M. Aspelmeyer, Proc. Natl. Acad. Sci. U.S.A. **108**, 16182 (2011).
 [7] R. Riedinger, S.k. Hong, R.A. Norte, J.A. Slater, J.Y. Shang, A.G. Krause, V. Anant, M. Aspelmeyer, and S. Groblacher, Nature, **530**, 313 (2016).
 [8] C. Galland, N. Sangouard, N. Piro, N. Gisin, and T.J. Kippen-

- berg, Phys. Rev. Lett. **112**, 143602 (2014).
- [9] A. Imamoglu, H. Schmidt, G. Woods, and M. Deutsch, Phys. Rev. Lett. **79**, 1467(1997).
- [10] I. Carusotto and C. Ciuti, Rev. Mod. Phys., **85**, 299 (2013).
- [11] N. Didier, S. Pugnetti, Y.M. Blanter, and R. Fazio, Phys. Rev. B **84**, 054503 (2011).
- [12] Y.X. Liu, A. Miranowicz, Y.B. Gao, J. Bajer, C.P. Sun, and F. Nori, Phys. Rev. A **82**, 032101 (2010).
- [13] A. Miranowicz, J. Bajer, N. Lambert, Y.X. Liu, and F. Nori, Phys. Rev. A **93** 013808 (2016).
- [14] X.W. Xu, A.X. Chen, and Y.X. Liu, Phys. Rev. A **94**, 063853 (2016).
- [15] H. Seok, and E.M. Wright, Phys. Rev. A **95**, 053844 (2017).
- [16] H.W.Ch. Postma, I. Kozinsky, A. Husain, and M.L. Roukesa, Appl. Phys. Lett. **86**, 223105 (2005).
- [17] V. Peano, and M. Thorwart, New J. Phys. **8**, 21 (2006).
- [18] E. Babourina-Brooks, A. Doherty, and G.J. Milburn, New J. Phys. **10**, 105020 (2008).
- [19] I. Katz, A. Retzker, R. Straub, and R. Lifshitz, Phys. Rev. Lett. **99**, 040404 (2007).
- [20] T.C.H. Liew, and V. Savona, Phys. Rev. Lett. **104**, 183601 (2010).
- [21] X.W. Xu, and Y.J. Li, J. phys. B: At. Mol. Opt. Phys. **46**, 035502 (2013).
- [22] D. Gerace, and V. Savona, Phys. Rev. A **89**, 031803(R) (2014).
- [23] M. Bamba, A. Imamoglu, I. Carusotto, and C. Ciuti, Phys. Rev. A **83**, 021802(R) (2011).
- [24] P. Komar, S.D. Bennett, K. Stannigel, S.J. M. Habraken, P. Rabl, P. Zoller, and M.D. Lukin, Phys. Rev. A **87**, 013839 (2013).
- [25] S. Etaki, M. Poot, I. Mahboob, K. Onomitsu, H. Yamaguchi, and H.S. van der Zant, Nature Phys. **4**, 785 (2008).
- [26] A. Andre et al., Nature Phys. **2**, 636 (2006).
- [27] K. Srinivasan, and O. Painter, Nature (London) **450**, 862 (2007).
- [28] T. Faust, J. Rieger, M.J. Seitner, J.P. Kotthaus, and E.M. Weig, Nat. Phys. **9**, 485 (2013).
- [29] H. Okamoto, A. Gourgout, C.Y. Chang, K. Onomitsu, I. Mahboob, E.Y. Chang, and H. Yamaguchi, Nat. Phys. **9**, 480 (2013).
- [30] J. Chan, A.H. Safavi-Naeini, J.T. Hill, S. Meenehan, and O. Painter, Appl. Phys. Lett. **101**, 081115 (2012).
- [31] A. Faraon, A. Majumdar, and J. Vuckovic, Phys. Rev. A **81**, 033838 (2010).
- [32] A. Li, T. Chen, Y.H. Zhou, and X.B. Wang, Opt. Lett. **41**, 1921-1924 (2016).
- [33] A. Li, T. Chen, Y.H. Zhou, and X.B. Wang, Opt. Lett. **41**, 1921 (2016).
- [34] M. J. Collett, and C.W. Gardiner, Phys. Rev. A **30**, 1386 (1984).
- [35] H. Flayac, and V. Savona, Phys. Rev. A **88**, 033836 (2013).
- [36] J.D. Cohen, S.M. Meenehan, G.S. Maccabe, S. Groblacher, A.H. Safavi-Naeini, F. Marsili, M.D. Shaw, and O. Painter, Nature, **520**, 522-525 (2015).